Magnetic Response of Mesoscopic Superconducting Rings with Two Order Parameters

Hendrik Bluhm,[1,*] Nicholas C. Koshnick,[1] Martin E. Huber,[2] and Kathryn A. Moler[1]

[1]*Departments of Physics and Applied Physics, Stanford University, Stanford, California 94305, USA*
[2]*Department of Physics, University of Colorado at Denver, Denver, Colorado 80217, USA*

(Received 11 August 2006; published 4 December 2006)

The magnetic response and fluxoid transitions of superconducting aluminum rings of various sizes, deposited under conditions likely to generate a layered structure, show good agreement with a two-order-parameter Ginzburg-Landau model. For intermediate couplings, we find metastable states that have different phase winding numbers around the ring in each of the two order parameters. Those states, previously theoretically predicted, are analogous to fractional vortices in singly connected samples with two-order-parameter superconductivity. Larger coupling locks the relative phase so that the two order parameters are only manifest in the temperature dependence of the response. With increasing proximitization, this signature gradually disappears.

DOI: 10.1103/PhysRevLett.97.237002 PACS numbers: 74.78.Na, 74.20.De, 74.45.+c, 74.78.Fk

Since the discovery of two-gap superconductivity in MgB_2 [1], the coexistence of two not-too-strongly coupled superconducting order parameters (OPs) has motivated significant theoretical work. A striking prediction is the existence of vortices carrying unquantized flux [2,3]. For non-negligible Josephson coupling, those exhibit a soliton-shaped phase difference between the two OPs [2,4]. Theoretically, such solitons may also form when current flow along a wire causes the relative phase to unlock, leading to a higher current than in the phase locked state [5]. Most of this theoretical work is based on a two-OP Ginzburg-Landau (GL) theory [6]. In the realm of superconductivity, this model applies for both Josephson-coupled bilayer systems, which are described microscopically by a tunneling BCS Hamiltonian, and intrinsic two-gap systems [7]. A particularly interesting example of the latter is Sr_2RuO_4. Its $p_x + ip_y$ OP would imply zero energy core excitations with non-Abelian braiding statistics, which have been envisioned as a basis for topologically protected quantum computation [8,9]. A similar two-OP model has also been used to describe a liquid metallic state of hydrogen [10], where the electrons and protons would form two independent superfluids.

Compared to the large number of theory papers, there is little experimental work on the mesoscopic structure of such two-OP systems. In this Letter, we report the observation of soliton states and other phenomena arising from the interplay between two OPs in quasi-1D, superconducting rings consisting of two parallel, Josephson-coupled aluminum layers. Positioning a scanning SQUID microscope [11] over each ring individually enabled measurements of the current, I, circulating the ring as a function of applied flux, Φ_a, and temperature, T. The ensemble of magnetic responses includes distinct features that cannot be explained by one-OP GL, but can be described by numerical solutions of two-OP GL. The inferred coupling between the two OPs depends on the ring's annulus width, w, allowing us to study the crossover between intermediate and strong coupling regimes. For intermediate coupling, we find metastable states with different phase winding numbers for each OP. Those are the 1D analogue of unquantized vortices [2], and imply a soliton-shaped phase difference [4]. In this regime, multiple transition pathways between states give a rich structure of hysteretic Φ_a-I curves. At stronger coupling, the system approaches the Cooper limit of complete proximitization [12]: the Φ_a-I curves at any temperature can be described by one-OP GL, but the existence of two OPs is manifest in the temperature dependence of the fitted penetration depth, λ, and the GL-coherence length, ξ_{GL}.

During a single, two-month-long cooldown, we characterized the magnetic response of 40 different rings with eight annulus widths 45 nm $\leq w \leq$ 370 nm and radii R of 0.5, 0.8, 1.2, and 2 μm. The rings were fabricated on oxidized silicon, using liftoff lithography with poly(methyl methacrylate) (PMMA) resist. The 40 nm thick Al film was deposited by e-beam evaporation at a rate of about 1 Å/s and a pressure of approximately 10^{-6} mbar. During the deposition, the rate temporarily dropped to a negligible level for about 10 min and subsequently recovered, which most likely caused the formation of two superconducting layers separated by an AlO_x tunneling barrier. A disk with a radius of 2 μm had a T_c of 1.6 K, representative of the bulk film. Using $\xi_0 = 1.6$ μm for pure bulk Al [13] and $\xi_{GL}(0) \approx 70$ nm for our rings, as derived below, we infer a mean free path of $l_e = 1.4\xi_{GL}(0)^2/\xi_0 = 4$ nm. The measured critical temperatures T_c of the rings ranged from 1.5 to 1.9 K, depending only on w. Both the short l_e and the large T_c compared to clean bulk Al indicate small grains and a (likely related) strong effect of oxygen impurities [14,15].

Our SQUID sensor has two counterwound pickup loops and field coils that are used to apply a local magnetic field [16]. We position one pickup loop over a ring, record time traces of the SQUID response while sinusoidally varying Φ_a at a few Hz, and average hundreds to thousands of field sweeps. A background, measured by retracting the SQUID from the sample, is subtracted. The remaining signal is the

flux generated by I, plus a residual, elliptic sensor background which is negligible at lower T and unambiguously distinguishable from the ring response at higher T, where fluxoid transitions occur. Details on the technique will be given elsewhere [17].

Rings with $w \leq 120$ nm show no two-OP effects. At low T [Fig. 1(a)], there are no fluxoid transitions at the experimental time scale and field sweep amplitude. At higher T [Figs. 1(b) and 1(c)], we observe hysteretic transitions, which become nonhysteretic near T_c [Fig. 1(d)].

We obtain the theoretical Φ_a-I curve of an individual fluxoid state, n, directly from 1D, one-OP GL [18]:

$$I_n(\varphi) = -\frac{wd\Phi_0}{2\pi R\mu_0\lambda^2}(\varphi - n)\left[1 - \frac{\xi_{\mathrm{GL}}^2}{R^2}(\varphi - n)^2\right], \quad (1)$$

where $\varphi = \Phi_a/\Phi_0$, $\Phi_0 = h/2e$, and d is the total film thickness. n is the phase winding number of the GL-OP $\psi(x) = |\psi|e^{inx/R}$, where x is the position along the ring's circumference. $\varphi - n \ll R/\xi_{\mathrm{GL}}$ gives the linear response of the London limit, while the cubic term arises from pair breaking. Because $wd \ll \lambda^2$, the self-inductance can be neglected. Although the width of some rings is several ξ_{GL} at low T, the 1D approximation is justified here because $w \ll R$ and $H_a \ll H_{c2}$ [18].

Close to T_c [Fig. 1(d)], transitions are fast enough to model the experimental Φ_a-I curves as a thermal average over all possible states,

$$\langle I(\varphi)\rangle = \frac{\sum_n I_n(\varphi)e^{-E_n(\varphi)/k_BT}}{\sum_n e^{-E_n(\varphi)/k_BT}}, \quad (2)$$

with $E_n(\varphi) = -\Phi_0\int_n^\varphi d\varphi' I_n(\varphi')$. We set $\xi_{\mathrm{GL}} = 0$ when substituting Eq. (1) into Eq. (2) because the thermal rounding dominates the cubic term [19]. The free parameters in the fit are λ^{-2}, three background parameters, a small offset in φ, the pickup loop–ring inductance M_{coup}, and the field coil–ring inductance. The fitted inductances are consistent with less accurate geometrical estimates and are used at lower T.

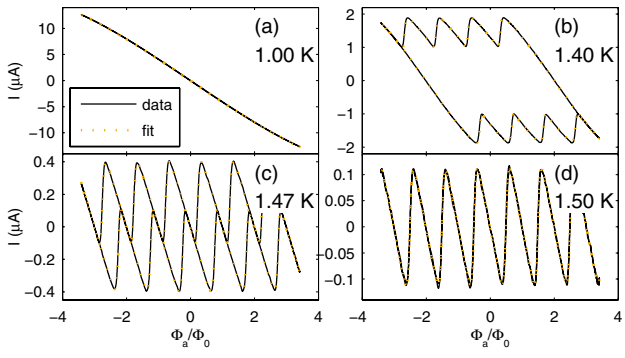

FIG. 1 (color online). Φ_a-I curves for a ring with $w = 120$ nm and $R = 1.2$ μm, fitted to a one-order-parameter Ginzburg-Landau model. The selected curves represent the regimes discussed in the text: (a) no transitions, (b),(c) hysteretic, and (d) thermal equilibrium.

The hysteretic curves [Figs. 1(b) and 1(c)] are rounded from averaging over a distribution of thermally activated transitions [21] near a typical $\varphi = \phi_t + n$. We model them by combining Eq. (1) with occupation probabilities $p_n(\varphi - n)$ obtained from integrating the rate equation $dp_n/dt = -p_n/\tau_0 \exp[-E_{\mathrm{act}}(\varphi - n)/k_BT]$. For fitting, τ_0 and the activation energy E_{act} are absorbed into ϕ_t. The free parameters are ϕ_t, $dE_{\mathrm{act}}/d\varphi(\phi_t)$, ξ_{GL}, λ^{-2}, and three background parameters. φ_t increases very weakly with increasing field sweep frequency, as expected for thermally activated behavior.

For $T \ll T_c$, where no transitions are seen, Eq. (1) fits the data with three parameters corresponding to ξ_{GL}, λ^{-2}, and a constant background.

The above models result in excellent fits for measured Φ_a-I curves except at $w = 190$ nm as discussed below. The fitted values for λ^{-2} and ξ_{GL} are shown in Fig. 2 for rings typical of each w. All 14 measured rings with $w \leq 120$ nm show T dependence similar to the one-OP phenomenological expressions $\lambda(T)^{-2} = \lambda(0)^{-2}(1 - t^4)$ and $\xi_{\mathrm{GL}}(T) = \xi_{\mathrm{GL}}(0)\sqrt{(1 + t^2)/(1 - t^2)}$, with $t = T/T_c$. For $w \geq 190$ nm, $\lambda^{-2}(T)$ has a high-temperature tail to an enhanced T_c and a peak in ξ_{GL} near but below T_c. Both effects are most pronounced at $w = 190$ nm. The Φ_a-I curves remain hysteretic well into the tails, showing that the enhanced T_c is not a fluctuation effect.

The most striking features of the Φ_a-I curves for a $w = 190$ nm ring [Figs. 3(a)–3(f)], typical for all six measured rings with $w = 190$ nm and $R \geq 0.8$ μm [22], are transi-

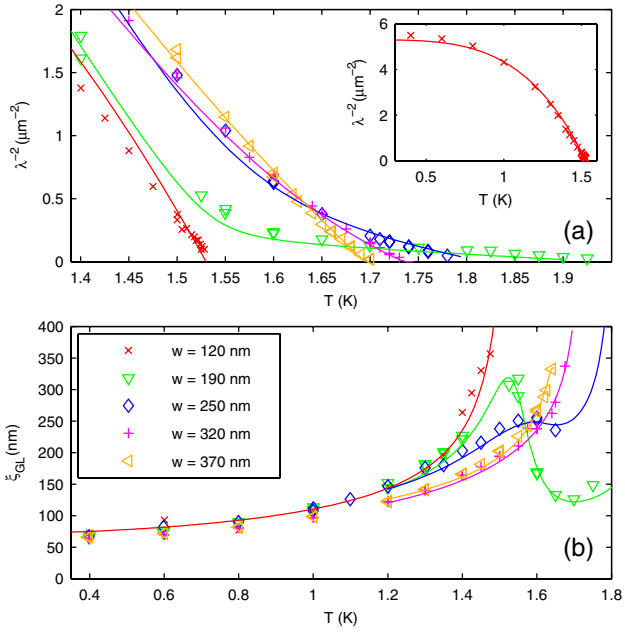

FIG. 2 (color online). (a) λ^{-2} and (b) ξ_{GL} for rings representative of each annulus width w. The discrete symbols are obtained from fits to Φ_a-I curves. Continuous curves represent fits to phenomenological expressions ($w = 120$ nm) or the two-order-parameter GL model ($w \geq 190$ nm), which was only fitted above 1.2 K where GL applies.

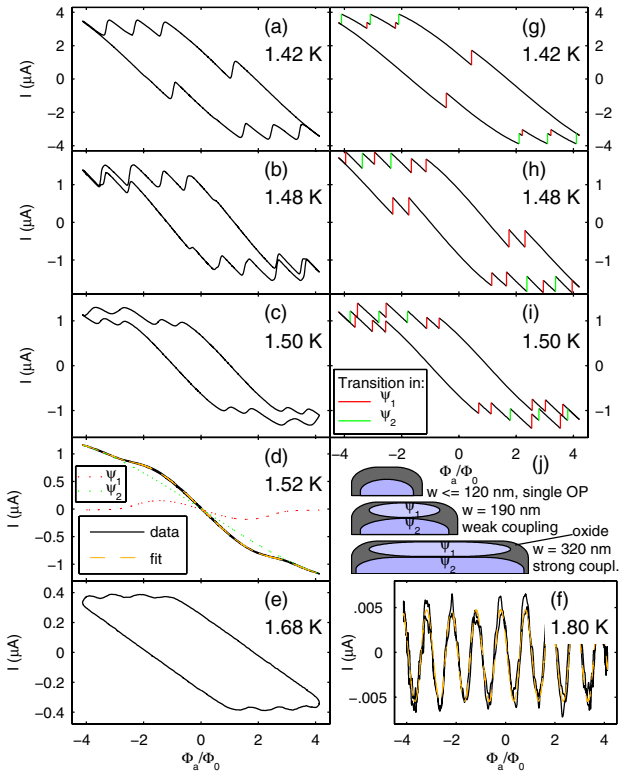

FIG. 3 (color online). (a)–(f) $\Phi_a - I$ curves for a ring with $w = 190$ nm and $R = 2$ μm, where the coupling between the two order parameters is weak. In (a)–(c), states with two different fluxoid numbers lead to the observed transition pattern. In (d), no transition occurs because one component is stabilized by the other. Dotted lines show the contributions of ψ_1 and ψ_2 derived from the model. (e) and (f), taken above the lower T_c, reflect the response of a single order parameter. (g)–(i) Results from the two-OP model corresponding to (a)–(c). (j) Schematic of film structure (cross section).

tion points in the lower T hysteretic region that are not a function of $\varphi - n$ only, and reentrant hysteresis. The latter is qualitatively related to the local maximum in $\xi_{\mathrm{GL}}(T)$ [Fig. 2(b)], since in one-OP GL, a state becomes unstable at $|\varphi - n| \geq \sqrt{R^2/\xi_{\mathrm{GL}}^2 + 1/2}/\sqrt{3}$ [23]. However, rather than an increase of the transitions point ϕ_t upon raising T, as expected for a decreasing $\xi_{\mathrm{GL}}(T)$, the amplitude of those transitions is reduced until a nonhysteretic curve with a flattening too pronounced to be described by Eq. (1) [Fig. 3(d)] appears. With a further increase of T [Figs. 3(e) and 3(f)], this flattening also disappears and the Φ_a-I curves evolve similarly to Fig. 1. This strongly suggests the existence of two OPs, one causing the small ripples in Fig. 3(c), and one with a larger T_c adding the large background response and causing the tail in $\lambda^{-2}(T)$. The additional phase winding number from a second, coupled OP also explains the irregular transitions in Figs. 3(a)–3(c). Although also breaking strict flux periodicity, finite line width corrections to 1D, one-OP GL [18] would be much smaller and more regular. A vortex pinned in the annulus could in principle lead to similar Φ_a-I curve; however, w is too small compared to ξ_{GL} to accommodate its core, and it cannot explain the T dependence of λ^{-2} and ξ_{GL}.

A two-OP GL model consisting of two standard 1D GL free energy functionals and a coupling term indeed reproduces the peculiar features of Figs. 2 and 3:

$$F[\psi_1, \psi_2, \varphi] = F_1[\psi_1, \varphi] + F_2[\psi_2, \varphi] + \frac{\gamma w}{2} \int_0^L dx |\psi_1 - \psi_2|^2, \tag{3}$$

with

$$F_i[\psi_i, \varphi] = w d_i \int_0^L dx \left\{ \frac{\hbar^2}{2m} \left| \left(-i\nabla + \frac{\varphi}{R} \right) \psi_i \right|^2 + \frac{\alpha_i}{2} |\psi_i|^2 + \frac{\beta_i}{4} |\psi_i|^4 \right\}. \tag{4}$$

We define ψ_1 to have the lower T_c. If both components have the same n, one can make the usual ansatz $\psi_i(x) = |\psi_i| e^{inx/R}$. Minimizing (3) with respect to $|\psi_1|$ and $|\psi_2|$ results in excellent fits to Φ_a-I curves as in Fig. 3(d). At small φ, both OPs contribute significantly, but as φ is increased, pair breaking strongly reduces $|\psi_1|$, whose ξ_{GL} diverges near $T_{c,1}$. In the absence of the more stable ψ_2, ψ_1 would undergo a fluxoid transition much before $|\psi_1|$ could be suppressed that much.

We extracted effective values of $\lambda^{-2}(T)$ and $\xi_{\mathrm{GL}}(T)$ from such modeled Φ_a-I curves [and also from fits to data sets similar to Fig. 3(d)] using a small φ expansion analogous to Eq. (1). Assuming a linear T dependence of α_1 and α_2, this procedure can reproduce the observed form of $\lambda^{-2}(T)$ and $\xi_{\mathrm{GL}}(T)$ as demonstrated by the fits in Fig. 2. The knee in $\lambda^{-2}(T)$ corresponds to the lower $T_{c,1}$, above which the amplitude of ψ_1 becomes very small. From $w = 190$ nm to $w = 370$ nm, the coupling strength γ increases by a factor 30–50, by far the largest line width dependence of all fit parameters [24]. The resulting stronger proximitization smears out the two-OP features. It appears that ψ_1 not only has a lower T_c, but also a smaller l_e than ψ_2. Fit parameters obtained from Φ_a-I curves and the curves in Fig. 2 are consistent within about a factor 2. This discrepancy may be due to fluctuations of ψ_1 at large φ or a nontrivial phase difference [5], which are not considered in our model for Φ_a-I curves.

To model the hysteretic Φ_a-I curves [Figs. 3(a)–3(c)], we calculate the activation energies $E_{\mathrm{act}}(\varphi - n)$ for transitions in either ψ_1 or ψ_2 by numerically computing saddle point solutions of the GL equations obtained from variation of (3), assuming that the relevant saddle points evolve continuously from those of the uncoupled system upon increasing γ. We then derive the complete Φ_a-I curve assuming that a transition in ψ_i occurs whenever $E_{\mathrm{act}}(\varphi - n) < \kappa_i k_B T$, where the $\kappa_{1,2}$ are treated as phenomenological parameters of order unity. Of several simulation runs with various parameters similar to those obtained from the fits, the one shown in Figs. 3(g)–3(i) gave the best simi-

larity with the data [Figs. 3(a)–3(c)]. While the uncertainty of the fit parameters [24] and simplicity of the model forbid a more quantitative comparison, the simulations show that metastable states with $n_1 \neq n_2$ are key to understanding the observed Φ_a-I curves. Because of the coupling between the OPs, the variation of the relative phase is soliton-like [4], similar to a Josephson vortex, however with the phase gradient along the junction being mostly due to the kinetic rather than the magnetic inductance. This soliton corresponds to the domain walls originating from unquantized vortices in bulk samples [2]. Intuitively, it is formed upon increasing φ when the larger ξ_{GL} of ψ_1 causes ψ_1 to become unstable at a smaller φ than ψ_2, and the coupling is weak enough for ψ_2 to stay in the same state. However, the soliton energy makes it less stable than states with $n_1 = n_2$. This leads to the observed steplike transition sequence.

Apart from the general agreement with the simulations and the irregular transitions, the most direct experimental evidence for states with $n_1 \neq n_2$ are branches of Φ_a-I curves that are shifted relative to each other by less than one Φ_0 horizontally, such as around $\Phi_a/\Phi_0 \approx \pm 3$ in Fig. 3(b). Individual, unaveraged field sweeps show that this is not an effect of averaging over different transition pathways, contrary to the features at $\Phi_a/\Phi_0 \approx \pm 0.3$.

The emergence of two OPs can be explained by the temporary drop of the deposition rate during the metalization. At the lower rate, more oxygen was codeposited to form a tunneling barrier [see Fig. 3(j)]. Different oxygen concentrations and/or grain sizes led to different values of T_c and ξ_{GL} in the two superconducting layers. It is known that PMMA outgases significantly and that thinner lines are affected more [25]. This likely caused the line width dependence of the coupling and the complete oxidization of one of the superconducting layers for $w \leq 120$ nm, where we found no evidence for two OPs. The critical Josephson current densities estimated from the inferred values of γ support this picture [24].

This fabrication result was unintentional but fortuitous. While the parameters should be tunable *a priori* with controlled exposure to oxygen gas, it would be difficult to obtain reproducible results from outgasing resist. Nevertheless, the data and analysis draw a clear picture of a two-OP superconductor with GL parameters that depend consistently on w. This dependence and the occurrence of two different T_c's allowed the study of a wide range of parameters. The insight thus gained may be used to design similar experiments on intrinsic two-component superconductors. The creation and detection of $h/4e$ vortices in Sr_2RuO_4 would be of particular interest [8,9]. Since their energy is logarithmically or linearly divergent in the sample size [2,3], they might only be accessible as metastable states in mesoscopic samples, similar to the soliton states discussed here.

In conclusion, we have explored effects emerging from two coupled order parameters in mesoscopic superconducting rings. The most interesting ones are an anomalous temperature dependence of the average superfluid density λ^{-2} and effective coherence length ξ_{GL}, and a qualitative modification of the behavior of phase slips related to previously predicted metastable states with two different phase winding numbers [2,5] and a soliton-shaped phase difference [4].

This work was supported by NSF Grants No. DMR-0507931, No. DMR-0216470, No. ECS-0210877, and No. PHY-0425897 and by the Packard Foundation. Work was performed in part at the Stanford Nanofabrication Facility, which is supported by NSF Grant No. ECS-9731293, its lab members, and industrial affiliates. We would like to thank Per Delsing, Egor Babaev, and Mac Beasley for useful discussions.

*Electronic address: hendrikb@stanford.edu

[1] C. Buzea and T. Yamashita, Supercond. Sci. Technol. **14**, R115 (2001).
[2] E. Babaev, Phys. Rev. Lett. **89**, 067001 (2002).
[3] E. Babaev, Nucl. Phys. **B686**, 397 (2004).
[4] Y. Tanaka, Phys. Rev. Lett. **88**, 017002 (2002); note that an error in the boundary condition for a ring geometry leads to some unphysical conclusions.
[5] A. Gurevich and V. M. Vinokur, Phys. Rev. Lett. **97**, 137003 (2006).
[6] A. Gurevich, Phys. Rev. B **67**, 184515 (2003).
[7] C. Noce and L. Maritato, Phys. Rev. B **40**, 734 (1989).
[8] M. Stone and S.-B. Chung, Phys. Rev. B **73**, 014505 (2006).
[9] S. Das Sarma, C. Nayak, and S. Tewari, Phys. Rev. B **73**, 220502(R) (2006).
[10] E. Babaev, A. Sudbo, and N. W. Ashcroft, Nature (London) **431**, 666 (2004).
[11] P. G. Bjornsson *et al.*, Rev. Sci. Instrum. **72**, 4153 (2001).
[12] P. G. D. Gennes, Rev. Mod. Phys. **36**, 225 (1964).
[13] R. Meservey and B. B. Schwartz, *Equilibrium Properties: Comparison of Experimental Results with Predictions of the BCS Theory* (Marcel Dekker, Inc., New York, 1969), pp. 117–84.
[14] R. B. Pettit and J. Silcox, Phys. Rev. B **13**, 2865 (1976).
[15] R. W. Cohen and B. Abeles, Phys. Rev. **168**, 444 (1968).
[16] M. E. Huber *et al.* (unpublished).
[17] N. C. Koshnick *et al.* (unpublished).
[18] X. Zhang and J. C. Price, Phys. Rev. B **55**, 3128 (1997).
[19] Fluctuation effects within a few mK of T_c [20], where it would be inadequate to set $\xi_{GL} = 0$, will be discussed in Ref. [17].
[20] F. von Oppen and E. K. Riedel, Phys. Rev. B **46**, 3203 (1992).
[21] J. S. Langer and V. Ambegaokar, Phys. Rev. **164**, 498 (1967).
[22] For rings with $R = 0.5$ μm, Φ_a was too small to observe those features.
[23] D. Y. Vodolazov *et al.*, Phys. Rev. B **67**, 054506 (2003).
[24] See EPAPS Document No. E-PRLTAO-97-084648 for a discussion of the fit procedures and parameters. For more information on EPAPS, see http://www.aip.org/pubservs/epaps.html.
[25] P. Dubos *et al.*, J. Vac. Sci. Technol. B **18**, 122 (2000).